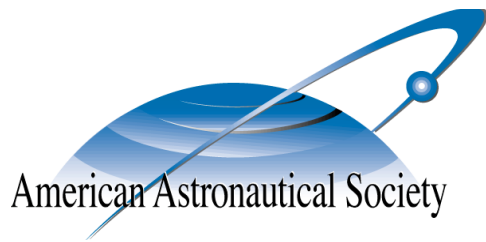


AAS 06-116



# APPROXIMATIONS OF DISTANT RETROGRADE ORBITS FOR MISSION DESIGN

Anil N. Hirani and Ryan P. Russell

## 16<sup>th</sup> AAS/AIAA Space Flight Mechanics Meeting

Tampa, Florida

January 22–26, 2006

AAS Publications Office, P.O. Box 28130, San Diego, CA 92198

# APPROXIMATIONS OF DISTANT RETROGRADE ORBITS FOR MISSION DESIGN

Anil N. Hirani \* and Ryan P. Russell †

Distant retrograde orbits (DROs) are stable periodic orbit solutions of the equations of motion in the circular restricted three body problem. Since no closed form expressions for DROs are known, we present methods for approximating a family of planar DROs for an arbitrary, fixed mass ratio. Furthermore we give methods for computing the first and second derivatives of the position and velocity with respect to the variables that parameterize the family. The approximation and derivative methods described allow a mission designer to target specific DROs or a range of DROs with no regard to phasing in contrast to the more limited case of targeting a six-state only.

## INTRODUCTION

Distant retrograde orbits (DROs) are a family of periodic orbit solutions of the equations of motion in the Circular Restricted Three Body Problem (CR3BP). The CR3BP is increasingly being used in mission design when a spacecraft is in the vicinity of two massive bodies like a planet and its moon and the effects of the two bodies on the spacecraft need to be taken into account. Recent examples of space missions heavily influenced by such multi-body effects are ISEE-3 (International Sun-Earth Explorer-3), ACE (Advanced Composition Explorer), SOHO (Solar and Heliospheric Observatory), and Genesis among others.<sup>1,2,3,4,5</sup>

By *family of DROs* we mean the DROs around a body, usually the moon of a planet, for a specific pair of bodies in CR3BP. We will consider planar DROs, most of which are extremely stable. Some examples of DROs in the CR3BP are shown in Figure 1. To place a spacecraft into such an orbit, one method is to compute a DRO, pick a six-state lying on the orbit and target that with a trajectory design optimization program. However, it could be that entering the same DRO at another state would have cost less. It could also be that a nearby DRO would have cost less while achieving a similar goal. In spacecraft trajectory design, such decisions are usually best left for an optimization program. Most optimization programs, at some level, use some kind of gradient descent. Thus they would need to compute derivatives of the states of a family of DROs with respect to the parameters. This paper addresses the problem of parameterizing a family of DROs and computing first and second derivatives of the state variables with respect to the parameters.

## Motivation for approximation

There is no known closed form for the DRO solutions of the CR3BP. The DROs shown in Figure 1 were obtained with a numerical differential corrector using a scheme described later. Thus the DROs can initially only be described as a collection of discrete positions and velocities. However, an optimization program may need to determine the state and its derivatives at any point along the orbit, not just at the points that were generated by the numerical differential corrector stage.

One solution is to store all the discrete states for the entire family. When a state in between two discrete states on an orbit, or in between two orbits is required, the only way to obtain it is by approximating the solution between sampled points. Computing intermediate values by numerically solving the differential

\*Assistant Professor, Department of Computer Science, University of Illinois at Urbana-Champaign, 201 N. Goodwin Avenue, Urbana, IL 61801, <http://www.cs.uiuc.edu/hirani>, Email: [hirani@uiuc.edu](mailto:hirani@uiuc.edu), Phone: 217-333-2727.

†Systems Engineer, Jet Propulsion Laboratory, California Institute of Technology, 4800 Oak Grove Drive, M/S 301-140L, Pasadena, CA 91108, [Ryan.Russell@jpl.nasa.gov](mailto:Ryan.Russell@jpl.nasa.gov), Phone: 818-393-6245.

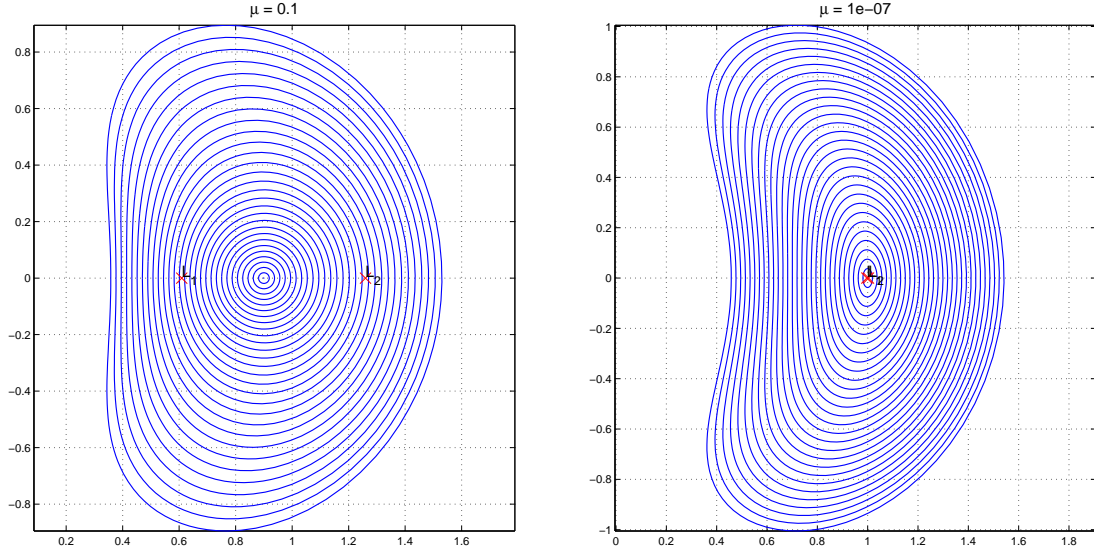


**Figure 1** Examples of DROs for two values of  $\mu$  in shown in rotating coordinates. The orbits are shown here around the smaller primary located at  $1 - \mu$ . The larger primary is at  $-\mu$ . DROs actually exist all the way to the other primary. A family of DROs also exists around the other primary. The  $L_1$  and  $L_2$  points are marked by a cross. On the right hand side at the scale of the figure the two libration points are almost overlapping.

equations each time or by using the differential corrector is not feasible. Derivatives at sample points can be computed using finite differences from which approximation to the derivatives can be obtained at intermediate points.

An alternative is to approximate the solution with a continuous function based on sampled states and dispense with the discrete data. The derivatives of the approximate orbits can be computed analytically and evaluation of derivatives can be programmed as a formula evaluation. This is the method we use in this paper. The approximate orbits will not necessarily be interpolating, i.e., the approximate orbit may not pass through the sample points exactly. But this may not matter in trajectory design. That's because as it is, the CR3BP is just a model. In actual mission design, the effects of many solar system bodies, gravitational potential due to non spherical shapes of bodies, solar pressure, and many other effects have to be taken into account. As far as trajectory design is concerned an added error due to orbit approximation may not matter, as long as it is small. This is true especially if the targeted family is very stable, as DROs are. The stability of DROs is discussed later. Exactly how much error can be tolerated can be judged by trajectory design studies using the full ephemeris and a high fidelity trajectory optimization software that uses our DRO approximation algorithms. Such a study has not yet been done. However, the algorithms discussed in this paper are demonstrated and proven useful for the phase-free targeting applications of several DROs in the Jupiter-Europa and the Earth-Moon systems.<sup>6</sup>

### Circular restricted three body model

For completeness we give here the equations of motion for the planar CR3BP. For derivations and more details see Reference 7. Consider two bodies (called the primaries) of masses  $m_1$  and  $m_2$  which orbit each other in a plane in circular orbits around their center of mass. The origin is at the center of mass. The third body is the spacecraft of mass so small that it does not affect the motion of the two primaries. Let  $\mu = m_2/(m_1 + m_2)$ . Now consider rotating coordinates, in which the origin is at the center of mass, and the two primaries lie along the  $x$ -axis. The mass  $m_1$  is at  $-\mu$  and  $m_2$  is at  $1 - \mu$ . If the spacecraft is in the

plane of the orbit of the primaries and if it has no  $z$ -component of velocity then the equations of motion for the spacecraft (the CR3BP equations) are :

$$\begin{aligned}\ddot{x} &= 2\dot{y} + x - \frac{(1-\mu)(x+\mu)}{r_1^3} - \frac{\mu(x-1+\mu)}{r_2^3} \\ \ddot{y} &= -2\dot{x} + y - \frac{(1-\mu)y}{r_1^3} - \frac{\mu y}{r_2^3}\end{aligned}\tag{1}$$

where  $r_1$  and  $r_2$  are the distances of the spacecraft from the two bodies, i.e.,

$$r_1 = ((x+\mu)^2 + y^2)^{1/2}\tag{2}$$

$$r_2 = ((x+\mu-1)^2 + y^2)^{1/2} .\tag{3}$$

The DROs such as those shown in Figure 1 are a family of periodic solutions of equation (1). The two families shown in Figure 1 are computed for two very different values of the parameter  $\mu$ .

### Stability of DROs

Most DROs are extremely stable. This can be seen, for example, by doing a linearized stability analysis of DROs which can be done by examining the eigenvalues of the monodromy matrix. A stability analysis that is more broadly applicable is one done with a dynamical systems tool like the Fast Lyapunov Indicator.<sup>8</sup> In Reference 9 this indicator was used to show that the family of DROs is the largest known region of stable orbits amongst all orbit families known for the CR3BP model. For other studies on the stability of DROs see References 10 and 11. For experimental studies using more realistic models see Reference 12.

To give some pictorial, numerical evidence of DRO stability, even when a realistic force model is used, we show Figure 6. This shows a comparison of a DRO in the CR3BP and in a more realistic model. The more realistic model uses gravity from all of the gas giants and all of the Galilean moons including spherical harmonic gravity terms at Europa ( $J_2$  and  $C_{22}$  terms) and Jupiter ( $J_2, J_3, J_4$  and  $J_6$  terms). From Figure 6 it can be seen that the orbit stays inside a band for very long times, an indication of the stability of this DRO, even in a realistic force model.

### Summary of our method and results

Since DROs are periodic, we use a truncated Fourier series approximation for modeling an individual orbit. To model a family we use polynomial interpolation of each coefficient over all the orbits. We then compute the derivatives explicitly and program them as function evaluations. Figure 4 shows the components of the state computed from the approximation scheme given in equations (8), (9) and (10). Figures 7, 8 and 9 show derivative computations resulting from our approximation scheme. Note that we only compute positions and velocities and their derivatives with respect to parameters. The time component is not important in the targeting application and is lost in the approximation process. The velocity can also be computed using the Jacobi constant (a constant of motion in CR3BP) and the position approximation in a way that is described later. While this is perhaps a more elegant approach to approximating the velocity, the derivative computations become significantly more complicated. We show preliminary results on velocity approximation using this idea in Figure 5.

## PARAMETERIZATION

For a given value of  $\mu$ , the positions of the states in the family of DROs about a primary can be globally parameterized by two variables. That is, there is a bijection between the set of all positions in the DRO family and a 2 parameter space to be described below and shown in Figure 2. Given a position on a particular orbit in the family, there is a unique point where that DRO crosses the the positive  $x$ -axis. There is also a unique angle measured counterclockwise from the positive  $x$ -axis to each point on a particular orbit. We will denote

these two quantities by  $r_p$  and  $\theta$  as shown in Figure 2. We will take the positive  $x$  direction to be  $\theta = 0$  and use  $(-\pi, +\pi]$  as the domain of values for  $\theta$ .

The mapping is invertible, i.e., any two numbers  $r_p > 0$  and  $-\pi < \theta \leq \pi$  determine a unique point on a particular orbit. We don't have proof for this latter invertibility condition but do have numerical evidence. This is evident for the example in Figure 2 since any radial ray drawn from the primary intersects a given orbit once. Thus the components of position and velocity of the orbits are functions of  $r_p$  and  $\theta$ , i.e. the functions  $x(r_p, \theta)$ ,  $y(r_p, \theta)$ ,  $\dot{x}(r_p, \theta)$  and  $\dot{y}(r_p, \theta)$  completely define the positions and velocities of a family of orbits for a given  $\mu$  value. As stated before, the time parameterization of the orbits in the family is lost in this representation but that is not an issue in the targeting application. The only thing that matters is the shape of the orbits and the velocity at each point on the orbits.

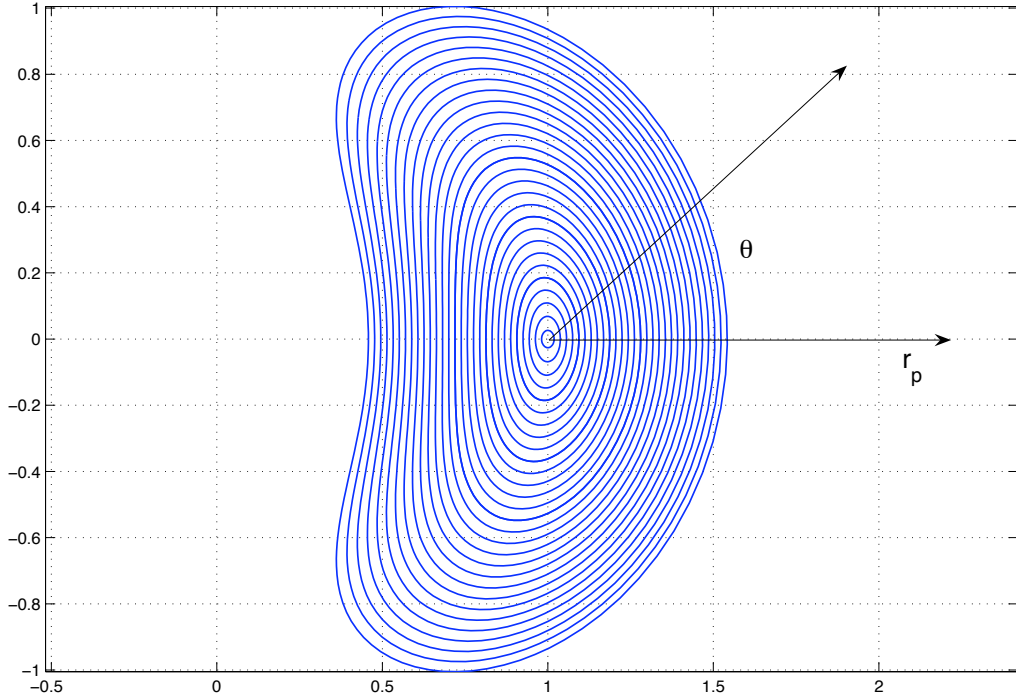


**Figure 2** Global parameterization of the family of DROs for a fixed value of  $\mu$ . We use  $r_p$  as one parameter and  $\theta$  as the other. The distance from the central primary to the positive  $x$ -crossing of a DRO is  $r_p$ . The origin is placed at the central primary. The angle measured from the positive  $x$ -axis to a point on a DRO is the  $\theta$  value in  $(-\pi, \pi]$  for that state.

## GENERATING THE DATA

There is no known closed form expression for the DRO solutions of the CR3BP. Therefore, we use a numerical differential corrector to obtain the orbits. This is the data that is then to be approximated for the purpose of optimal targeting. To start with, the differential corrector is given the initial conditions of a very small circular Keplerian orbit about a primary body at a point on the  $x$ -axis close to the primary. The orbit is propagated for one half-revolution. The corrector then makes minor adjustments to the initial conditions such that the encounter with the  $x$ -axis after the half-revolution is perpendicular. Due to symmetry, the resulting orbit will close after another half-revolution. We record the periodic orbit then repeat the process as we step outwards to the right along the  $x$ -axis.

For the next point along the  $x$ -axis, the previous initial condition is used as a starting guess for the differential corrector. We would like the data to be evenly spaced in the  $r_p$  and  $\theta$  parameter directions. For the  $r_p$

direction, we just step with a fixed sized gap when we move from one orbit to the next. To get even spacing in the  $\theta$  direction, once the differential corrector has found the initial conditions for an orbit, we divide the  $\theta$  direction in equal segments. Then we step through the orbit and interpolate to the exact  $\theta$  stopping points. In Figure 3 we show a sampling of raw position data for planar DROs around Europa in the Jupiter-Europa system. The initial points are on the positive  $x$ -axis and the initial velocity is always vertical and in the down direction. Since the orbits are symmetric w.r.t the  $x$ -axis we only need to go from 0 to  $-\pi$ . For more details on how the data is generated see Reference 11. For most of the experiments in this paper the data we used had 256 points in each orbit, equally spaced in  $\theta$  direction in  $[0, -\pi)$ .

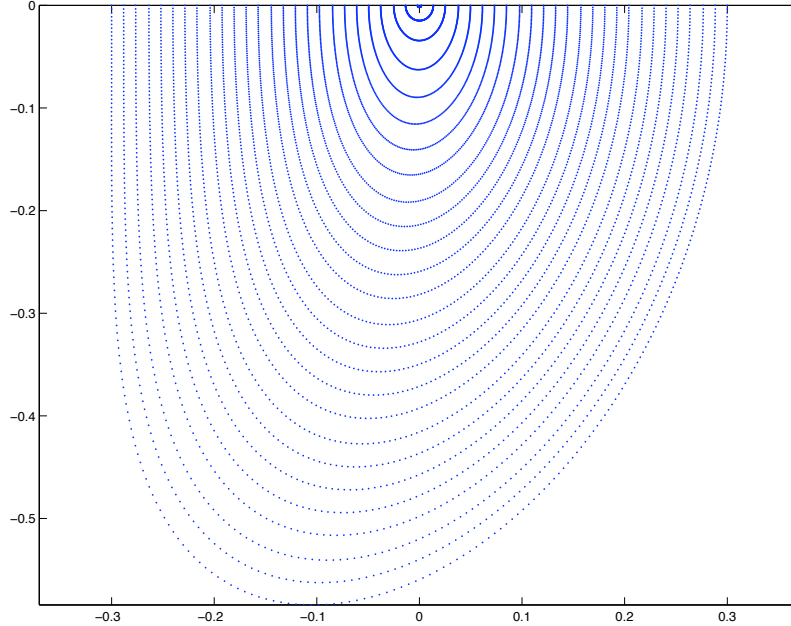


**Figure 3** A sampling of planar DROs around Europa in the Jupiter-Europa system, with  $\mu = 2.528 \times 10^{-5}$ . About 10% of the orbits generated are shown here. The origin is at Europa, and Jupiter is at -1. With the mean Jupiter-Europa distance of 671,000 km, the smallest  $r_p$  (positive  $x$ -crossing) of about 0.0018 corresponds to about 1208 km from Europa and the largest  $r_p = 0.3$  in the figure corresponds to about 201,300 km from Europa. The initial velocity is always vertical in the down direction. Since the orbits are symmetric w.r.t the  $x$ -axis we only need to go from 0 to  $-\pi$ . There were 256 such orbits generated with 256 points in each in  $[0, -\pi)$ .

## PROBLEM STATEMENT

Now we are ready to state the problem precisely. The data generated as described above is a table of values of  $x, y, \dot{x}$  and  $\dot{y}$  at the sampled values of  $r_p$  and  $\theta$ . The same values of  $\theta$  are used to generate the data for all the orbits. After the data has been generated, the starting point for the approximation process is a table for each component of the state. Each row of the table corresponds to the component's values in a single orbit with a unique  $r_p$  value. Each column corresponds to the component's values on different orbits that are encountered by a ray starting from origin and pointing in one of the sampled  $\theta$  directions.

We will refer to the table corresponding to a component by the uppercase letter. Thus the tables of values in the raw data are  $X, Y, \dot{X}$  and  $\dot{Y}$ . We will refer to the discrete values of  $r_p$  as  $r_i$  for  $1 \leq i \leq R$ . These are the values of  $r_p$  sampled by the data generation process. Similarly, the discrete values of  $\theta$  that are sampled

will be referred to as  $\theta_j$  for  $1 \leq j \leq T$ . To refer to a generic state component we will use  $q$  and refer to a generic state data table as  $Q$ , i.e.,  $q$  will stand for one of  $x, y, \dot{x}$  or  $\dot{y}$  and  $Q$  for one of  $X, Y, \dot{X}$  or  $\dot{Y}$ .

Each such table of data has to be approximated by a function of  $r_p$  and  $\theta$  that is at least twice differentiable. That is, from the tables of data, we would like to generate at least twice differentiable functions

$$x(r_p, \theta), \quad y(r_p, \theta), \quad \dot{x}(r_p, \theta), \quad \dot{y}(r_p, \theta) \quad (4)$$

such that

$$Q(i, j) \approx q(r_i, \theta_j)$$

for each state component  $q$ . Note that we do not require interpolation at the data points, and this gives us the freedom to use approximation schemes like Fourier series, which give excellent approximation for periodic functions without being interpolatory.

In addition, we would like to compute the first and second partial derivatives. That is, for each state component  $q(r_p, \theta)$  listed in (4), we would like to compute

$$\frac{\partial q}{\partial r_p}, \quad \frac{\partial q}{\partial \theta}, \quad \frac{\partial^2 q}{\partial r_p^2}, \quad \frac{\partial^2 q}{\partial \theta^2}, \quad \frac{\partial^2 q}{\partial r_p \partial \theta} \quad (5)$$

as functions of  $r_p$  and  $\theta$ . The basic requirement is that the functions in (4) and (5) above should be in closed form so they can be programmed as function evaluations for any valid  $r_p$  and  $\theta$  argument.

## APPROXIMATING A FAMILY OF DROS

Since the state component functions are periodic smooth functions of  $\theta$  and smooth functions of  $r_p$ , for a given  $r_p$  and  $\theta$  we can expand the component functions as Fourier series as follows:

$$\begin{aligned} x(r_p, \theta) &= \frac{a_0(r_p)}{2} + \sum_{m=1}^{\infty} a_m(r_p) \cos(n\theta) \\ y(r_p, \theta) &= \sum_{m=1}^{\infty} b_m(r_p) \sin(n\theta) \\ \dot{x}(r_p, \theta) &= \sum_{m=1}^{\infty} c_m(r_p) \sin(n\theta) \\ \dot{y}(r_p, \theta) &= \frac{d_0(r_p)}{2} + \sum_{m=1}^{\infty} d_m(r_p) \cos(n\theta). \end{aligned} \quad (6)$$

As is evident from Figure 1 and Reference 11, the orbits are symmetric w.r.t reflection about the  $x$ -axis. Thus the components of the position and velocity show the following relationships with respect to the  $\theta$  variable :

$$\begin{aligned} x(r_p, -\theta) &= x(r_p, \theta) \\ y(r_p, -\theta) &= -y(r_p, \theta) \\ \dot{x}(r_p, -\theta) &= -\dot{x}(r_p, \theta) \\ \dot{y}(r_p, -\theta) &= \dot{y}(r_p, \theta). \end{aligned}$$

That is,  $x$  and  $\dot{y}$  are even functions of  $\theta$  and  $y$  and  $\dot{x}$  are odd functions of  $\theta$ . This is why only cosine terms appear in the series for  $x$  and  $\dot{y}$  and only sine terms appear in the series for  $y$  and  $\dot{x}$  in (6). From the definition

of Fourier series,<sup>13</sup> we know that the coefficients that appear in (6) are defined as follows:

$$\begin{aligned}
a_m(r_p) &:= \frac{2}{\pi} \int_0^\pi x(r_p, \theta) \cos(n\theta) d\theta, \quad (m \geq 0) \\
b_m(r_p) &:= \frac{2}{\pi} \int_0^\pi y(r_p, \theta) \sin(n\theta) d\theta, \quad (m \geq 1) \\
c_m(r_p) &:= \frac{2}{\pi} \int_0^\pi \dot{x}(r_p, \theta) \sin(n\theta) d\theta, \quad (m \geq 1) \\
d_m(r_p) &:= \frac{2}{\pi} \int_0^\pi \dot{y}(r_p, \theta) \cos(n\theta) d\theta, \quad (m \geq 0).
\end{aligned} \tag{7}$$

We will get our approximations by using the tabular data  $X, Y, \dot{X}, \dot{Y}$ , to estimate a subset of the coefficients in (6). We first note that we can only store finitely many coefficients, and hence we will truncate the series that appear in equation (6), say at  $m = M$ . The definitions in (7) would still require the state functions that we are trying to approximate in the first place. We get around this problem by first replacing the integrals in (7) by a quadrature rule. Thus, we approximate the Fourier coefficients for each discrete  $r_p$  value as follows:

$$\begin{aligned}
a_m(r_i) &:= \frac{2}{\pi} \sum_{j=1}^{T-1} \frac{X(i, j+1) \cos(m\theta_{j+1}) + X(i, j) \cos(m\theta_j)}{2} (\theta_{j+1} - \theta_j), \quad (m \geq 0) \\
b_m(r_i) &:= \frac{2}{\pi} \sum_{j=1}^{T-1} \frac{Y(i, j+1) \sin(m\theta_{j+1}) + Y(i, j) \sin(m\theta_j)}{2} (\theta_{j+1} - \theta_j), \quad (m \geq 1) \\
c_m(r_i) &:= \frac{2}{\pi} \sum_{j=1}^{T-1} \frac{\dot{X}(i, j+1) \sin(m\theta_{j+1}) + \dot{X}(i, j) \sin(m\theta_j)}{2} (\theta_{j+1} - \theta_j), \quad (m \geq 1) \\
d_m(r_i) &:= \frac{2}{\pi} \sum_{j=1}^{T-1} \frac{\dot{Y}(i, j+1) \cos(m\theta_{j+1}) + \dot{Y}(i, j) \cos(m\theta_j)}{2} (\theta_{j+1} - \theta_j), \quad (m \geq 0)
\end{aligned} \tag{8}$$

where we have used trapezoidal rule to approximate the integrals and where  $1 \leq i \leq R$ . We approximate the coefficients  $a_m, b_m, c_m$  and  $d_m$  as smooth functions of  $r_p$  by using polynomial approximations. That is, we define :

$$\begin{aligned}
a_m(r_p) &:= \sum_{n=0}^N A(m, n) P_n(r_p) \\
b_m(r_p) &:= \sum_{n=0}^N B(m, n) P_n(r_p) \\
c_m(r_p) &:= \sum_{n=0}^N C(m, n) P_n(r_p) \\
d_m(r_p) &:= \sum_{n=0}^N D(m, n) P_n(r_p)
\end{aligned} \tag{9}$$

where  $m \geq 0$  for  $a_m$  and  $d_m$  and  $m \geq 1$  for  $b_m$  and  $c_m$ . The polynomials  $P_n, 0 \leq n \leq N$  used above are a basis for the set of polynomials in  $r_p$  of degree less than or equal to  $N$ . The data to be approximated by equation (9) is obtained from equation (8). Here  $A$  and  $D$  are  $(M+1) \times (N+1)$  matrices and  $B$  and  $C$  are  $M \times (N+1)$  matrices. These matrices encode the smooth approximation of a family of DROs. Finding these matrices is the goal of the approximation process.

Consider the coefficients  $A(m, n)$  (the procedure for finding others is the same). We can solve for these by first evaluating  $a_m(r_p)$  at the discrete values  $r_i, 1 \leq i \leq R$ , using equation (8). Then we do a one

dimensional curve fit to find the coefficients  $A(m, n)$ . For this paper we used Chebyshev polynomials as the basis polynomials  $P_n$ .

Now we can summarize our approximation scheme as follows. Define the state components by:

$$\begin{aligned}
x(r_p, \theta) &= (1/2) \sum_{n=0}^N A(0, n) P_n(r_p) + \sum_{m=1}^M \left( \sum_{n=0}^N A(m, n) P_n(r_p) \right) \cos(m\theta) \\
y(r_p, \theta) &= \sum_{m=1}^M \left( \sum_{n=0}^N B(m, n) P_n(r_p) \right) \sin(m\theta) \\
\dot{x}(r_p, \theta) &= \sum_{m=1}^M \left( \sum_{n=0}^N C(m, n) P_n(r_p) \right) \sin(m\theta) \\
\dot{y}(r_p, \theta) &= (1/2) \sum_{n=0}^N D(0, n) P_n(r_p) + \sum_{m=1}^M \left( \sum_{n=0}^N D(m, n) P_n(r_p) \right) \cos(m\theta)
\end{aligned} \tag{10}$$

where the coefficients  $A(m, n)$ ,  $B(m, n)$ ,  $C(m, n)$ , and  $D(m, n)$  are as defined by equation (8) and equation (9). Equation (10) shows how the smooth state component functions can be represented by finite sized matrices  $A$ ,  $B$ ,  $C$  and  $D$ . Figure 4 shows the state approximation when Chebyshev polynomials basis is used as the  $P_n$  polynomials in equations (9) and (10).

The state component functions of equation (10) involve polynomials in  $r_p$  and trigonometric functions of  $\theta$ . Computing the desired derivatives of these functions listed in (5) is straightforward and thus can be programmed as formula evaluations. This was done for the component functions shown in Figure 4. The resulting derivatives appear in Figures 7, 8 and 9. The results of the derivative computations are compared against a finite difference calculation at the sampled  $r_p$  and  $\theta$  values. This is just for testing our formulas for first and second derivatives. As mentioned before, the formula evaluation method has the advantage that the derivatives can be computed at any  $r_p$  and  $\theta$  values, unlike the finite difference computations which can only be done at the sampled points.

## JACOBI CONSTANT AND VELOCITY APPROXIMATIONS

In the previous section we have shown how to approximate the velocity when it is represented as a two component vector  $(\dot{x}, \dot{y})$ . We do this in equations (6) and (10) by using a separate truncated Fourier series for each of the 2 components. An alternative is to represent velocity with just one scalar variable. Since the velocity vector is tangential to the orbit, the direction of the velocity can be computed from the orbit curve in position space. To get the magnitude of the velocity vector at a point on a DRO we use the Jacobi constant of the orbit and the position of the point. The Jacobi constant is a constant of motion in CR3BP, i.e. it is constant along solutions of CR3BP equations.<sup>7</sup> Thus, each DRO has a single number as its Jacobi constant. As is usual, we will denote this constant by  $C$ . By definition,  $C = -2E$ , where  $E$  is an energy-like value defined as follows:

$$-\frac{C}{2} := E(x, y, \dot{x}, \dot{y}) := \frac{1}{2}(\dot{x}^2 + \dot{y}^2) - \frac{1}{2}(x^2 + y^2) - \frac{1-\mu}{r_1} - \frac{\mu}{r_2} \tag{11}$$

where  $r_1$  and  $r_2$  are as in equation (2).

We can treat the velocity norm as the unknown, use the fact that  $C$  is constant along a DRO, and rearrange equation (11) to get :

$$(\|\mathbf{v}\|(r_p, \theta))^2 = -C(r_p) + ((x(r_p, \theta))^2 + (y(r_p, \theta))^2) + \frac{2(1-\mu)}{r_1} + \frac{2\mu}{r_2}. \tag{12}$$

By  $\|\mathbf{v}\|(r_p, \theta)$  we mean that  $\|\mathbf{v}\|$  is a function of  $r_p$  and  $\theta$ . The Jacobi constant  $C(r_p)$  is computed from the data for the sampled data points by using equation (11). We compute it for the data of a DRO for every point

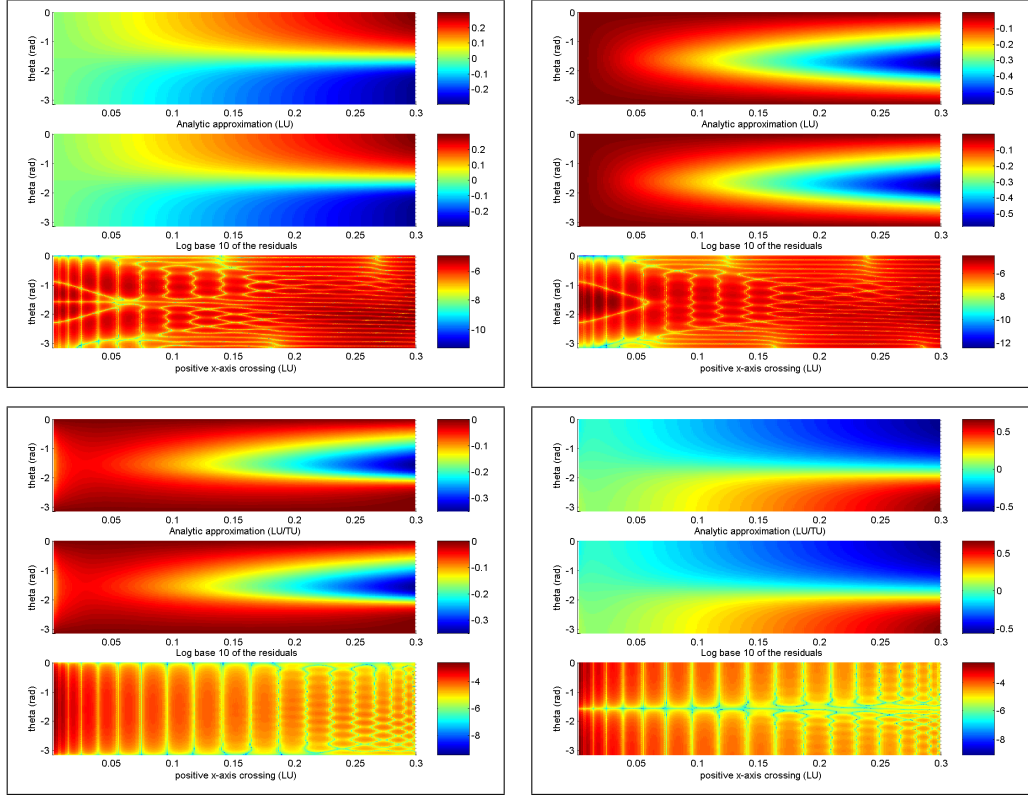


**Figure 4** Approximation of state component functions using Chebyshev polynomials to approximate Fourier coefficients of the series representing each orbit. The raw orbit data used for this figure is shown in Figure 3. The top two boxes show approximation of  $x$  and  $y$  and the bottom two for  $\dot{x}$  and  $\dot{y}$ . In each box the top plot is the data generated by the differential corrector, and the middle plot is the approximation obtained with equation (10) using Chebyshev polynomial basis. The third plot in each box shows the log base 10 of the absolute value of the residual at the sample points. The horizontal axis in each plot is  $r_p$  and the vertical axis is  $\theta$ . For this calculation 50 terms of Fourier series and up to degree 100 Chebyshev polynomials were used, i.e., in equation (10)  $M = 50$  and  $N = 100$ .

on it and take the average value to be the  $C$  value for that orbit. To get  $C(r_p)$  for arbitrary  $r_p$  we approximate the  $C$  values computed from the data by a polynomial. Thus given an  $r_p$  and  $\theta$  we can evaluate the polynomial  $C(r_p)$  and use equation (12) to compute the velocity norm at  $(r_p, \theta)$ . The unit tangent vector at  $(r_p, \theta)$  is:

$$\left( \frac{\partial x}{\partial \theta} \left/ \left\| \frac{\partial \mathbf{r}}{\partial \theta} \right\|, \frac{\partial y}{\partial \theta} \left/ \left\| \frac{\partial \mathbf{r}}{\partial \theta} \right\| \right) \right)$$

where  $\mathbf{r} = (x(r_p, \theta), y(r_p, \theta))$  is the position at  $(r_p, \theta)$  obtained from the approximations for  $x$  and  $y$  computed as in equation (10). Then finally, the velocity components can be computed as:

$$\begin{aligned} \dot{x}(r_p, \theta) &= (\|\mathbf{v}\|(r_p, \theta)) \frac{\partial x}{\partial \theta} \left/ \left\| \frac{\partial \mathbf{r}}{\partial \theta} \right\| \right. \\ \dot{y}(r_p, \theta) &= (\|\mathbf{v}\|(r_p, \theta)) \frac{\partial y}{\partial \theta} \left/ \left\| \frac{\partial \mathbf{r}}{\partial \theta} \right\| \right. . \end{aligned} \quad (13)$$

An example of velocity approximation using this method is shown in Figure 5. We have not yet used this method to compute the first and second derivatives of the positions and velocities. The presence of

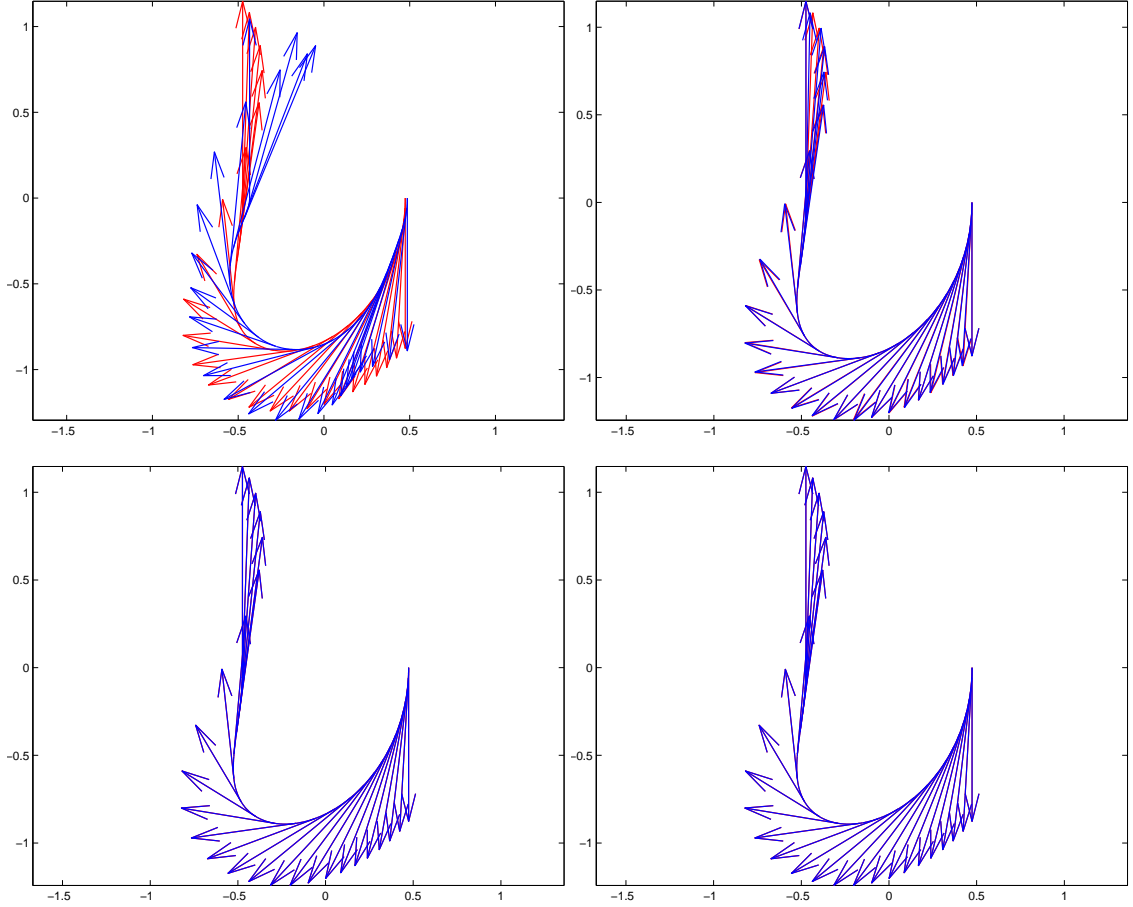


**Figure 5** Approximation of velocity using tangent vectors and Jacobi constant as given in equation (13) and (12). The arrows represent velocity at a point and are drawn to scale. Blue is data and red is approximation. From top to bottom, left to right: 4, 16, 32 and 64 terms of the Fourier series were used. With 32 and 64 terms of Fourier series (bottom row) the velocity vectors in the data and the smooth approximation almost lie on top of each other at the scale of the figure.

the norms in the denominators in equations (13) makes the analytical derivative computations complicated, especially for the second derivatives. We have implemented a Mathematica program to symbolically compute the derivatives and then automatically generate the corresponding numerical code. The resulting code has not yet been tested.

## ALTERNATIVES AND IMPROVEMENTS

In this paper we have shown methods for approximating the orbits using the same type of representation for all the orbits in the family. But note from Figure 1 that the orbits for a fixed  $\mu$  can be roughly divided into 4 domains. Very close to the primary (around which the orbit lies), the effects of the distant primary are small. As a result these small orbits are almost Keplerian circular orbits and can be accurately modeled using two body motion for short periods or Hill's approximations for longer periods.

Moving away from the smaller primary, there exists a region where the spacecraft is heavily influenced by both the primaries and the motion must be modeled using the CR3BP. Moving further away, the motion of the spacecraft is dominated by the other primary and is flying in formation with the effectively massless smaller

primary. The motion in this region is modeled well with the Clohessey-Wiltshire model until the distance to the smaller primary begins to violate the linearization approximations of the model. The DROs in this region take on the 2:1 ellipse shapes predicted by the Clohessey-Wiltshire model. Beyond this region, higher order terms are necessary to model the motion well as the orbits are no longer symmetric with respect to the y-axis and they take on a “kidney bean” shape.

While the motion in each of these regions is well approximated by the described models, the boundaries between regions can be difficult to define. For problems that require DROs in multiple regions, it is much simpler to approximate all of the motion using the CR3BP.

Even when the entire family is modeled using the CR3BP as we have done, there are other approximation schemes besides the ones we have described. For example, one can use Fourier series for the  $\theta$  direction as we have done, but use piecewise polynomials, such as splines, to approximate the Fourier coefficients in the  $r_p$  direction. Alternatively, one can use two dimensional spline patches to represent the components.

The computational cost for computing the approximations should be studied carefully. One possible improvement in speed can come from the use of the Fast Fourier Transform (or rather Discrete Cosine and Sine Transforms) to obtain the Fourier series representations of the state components.

## CONCLUSIONS

We have given a general method to parameterize DROs for any CR3BP system. We start with generating a discrete set of points on a family of DROs for a given  $\mu$  using a differential corrector. Each orbit in the family is approximated by a truncated Fourier series and the family is approximated by polynomial approximation of the Fourier series coefficients. The data approximation as well as the derivatives are of sufficient accuracy for targeting purposes. In targeting applications the smoothness and consistency of the data and derivatives is of more importance than the accuracy beyond a few digits. By definition our data is smooth and consistent. The DRO approximation scheme described here gives us a tool for mission design to optimally target phase-free DROs and families of phase-free DROs. This is a significant improvement to the existing capabilities, both in spacecraft performance and mission analyst design time.

## ACKNOWLEDGMENTS

We thank Larry Bright and Jon Sims for giving us the chance to work on this project. We also thank Try Lam, Jin Ma, Benjamin Villac and Greg Whiffen for suggestions. The research described in this paper was carried out at the Jet Propulsion Laboratory, California Institute of Technology, under contract with the National Aeronautics and Space Administration and at the University of Illinois at Urbana-Champaign.

## REFERENCES

- [1] R. Farquhar, D. Muhonen, C. Newman, and H. Heuberger, “Trajectories and Orbital Maneuvers for the First Libration Point Satellite,” *Journal of Guidance and Control*, Vol. 3, No. 6, 1980, pp. 549–554.
- [2] P. Sharer and T. Harrington, “Trajectory Optimization for the ACE Halo Orbit Mission, Paper AAS 96-3601,” *AAS/AIAA Astrodynamics Specialist Conference, San Diego, California*, American Astronautical Society and American Institute of Aeronautics and Astronautics, July 1996.
- [3] C. Roberts, “The SOHO Mission L1 Halo Orbit Recovery From the Attitude Control Anomalies,” *Libration Point Orbits and Applications Conference, Parador d’Aiguablava, Girona, Spain*, June 2002.
- [4] W. S. Koon, M. W. Lo, J. E. Marsden, and S. D. Ross, “The Genesis Trajectory and Heteroclinic Connections, Paper AAS 99-451,” *AAS/AIAA Astrodynamics Specialist Conference, Girdwood, Alaska*, American Astronautical Society and American Institute of Aeronautics and Astronautics, August 1999.
- [5] K. Howell, B. Barden, R. Wilson, and M. Lo, “Trajectory Design Using a Dynamical Systems Approach with Applications to Genesis, Paper AAS 97-709,” *AAS/AIAA Astrodynamics Specialist Conference, Sun Valley, Idaho*, American Astronautical Society and American Institute of Aeronautics and Astronautics, August 1997.
- [6] R. P. Russell, “Primer Vector Theory Applied to Global Low-Thrust Trade Studies, Paper AAS 06-156,” *16th AAS/AIAA Space Flight Mechanics Meeting, Tampa, Florida*, AAS/AIAA, 2006.

- [7] S. D. Ross, *Cylindrical manifolds and tube dynamics in the restricted three-body problem*. PhD thesis, California Institute of Technology, 2004.
- [8] B. F. Villac and J. J. Aiello, "Mapping Long-Term Stability Regions Using the Fast Lyapunov Indicator, Paper AAS 05-188," *AAS/AIAA Space Flight Mechanics Meeting, Copper Mountain, Colorado*, American Astronautical Society and American Institute of Aeronautics and Astronautics, January 2005.
- [9] M. Lara, R. P. Russell, and B. F. Villac, "On Parking Solutions Around Europa, Paper AAS 05-384," *AAS/AIAA Astrodynamics Specialist Conference, Lake Tahoe, California*, American Astronautical Society and American Institute of Aeronautics and Astronautics, August 2005.
- [10] M. Hénon, "Numerical exploration of the restricted problem. V. Hill's case: periodic orbits and their stability," *Astronomy and Astrophysics*, Vol. 1, 1969, pp. 223–238.
- [11] R. P. Russell, "Global search for planar and three-dimensional periodic orbits near Europa, Paper AAS 05-290," *AAS/AIAA Astrodynamics Specialist Conference, Lake Tahoe, California*, AAS/AIAA, 2005.
- [12] T. Lam and G. J. Whiffen, "Exploration of Distant Retrograde Orbits Around Europa, Paper AAS 05-115," *AAS/AIAA Space Flight Mechanics Meeting, Copper Mountain, Colorado*, American Astronautical Society and American Institute of Aeronautics and Astronautics, January 2005.
- [13] R. V. Churchill and J. W. Brown, *Fourier series and boundary value problems*. New York: McGraw-Hill Book Co., fourth ed., 1987.

**Note: 4 pages of figures follow this page.**

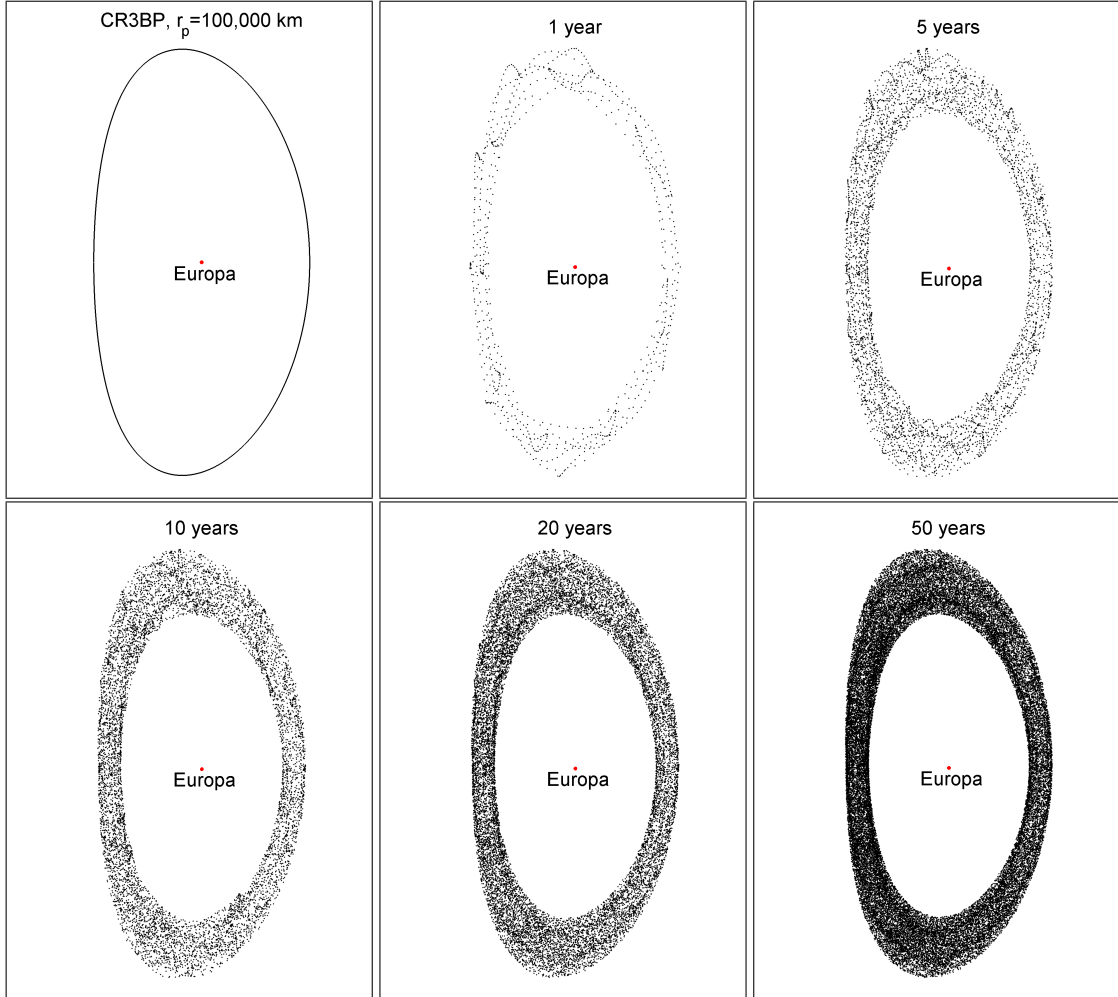


**Figure 6** Stability of DROs in realistic force models. Top left shows a DRO in the Jupiter-Europa system in the CR3BP model. The subsequent figures show what happens if an initial condition from the DRO is integrated with a more realistic model for 1, 5, 10, 20 and 50 years. The model for these integrations uses gravity from all of the gas giants and all of the Galilean moons including spherical harmonic gravity terms at Europa ( $J_2$  and  $C_{22}$  terms) and Jupiter ( $J_2$ ,  $J_3$ ,  $J_4$  and  $J_6$  terms). The band in the 50 year figure is about 60,000 km thick at the top and bottom and about 25,000 km thick at the sides. The band shrinks to a very narrow one if the DRO chosen is closer to Europa. In the realistic model integrations, it can be seen that the band fills up quickly and then the orbit stays in this band. In these figures, 10 dots are plotted per revolution, while the integrator takes about 100 steps per revolution.

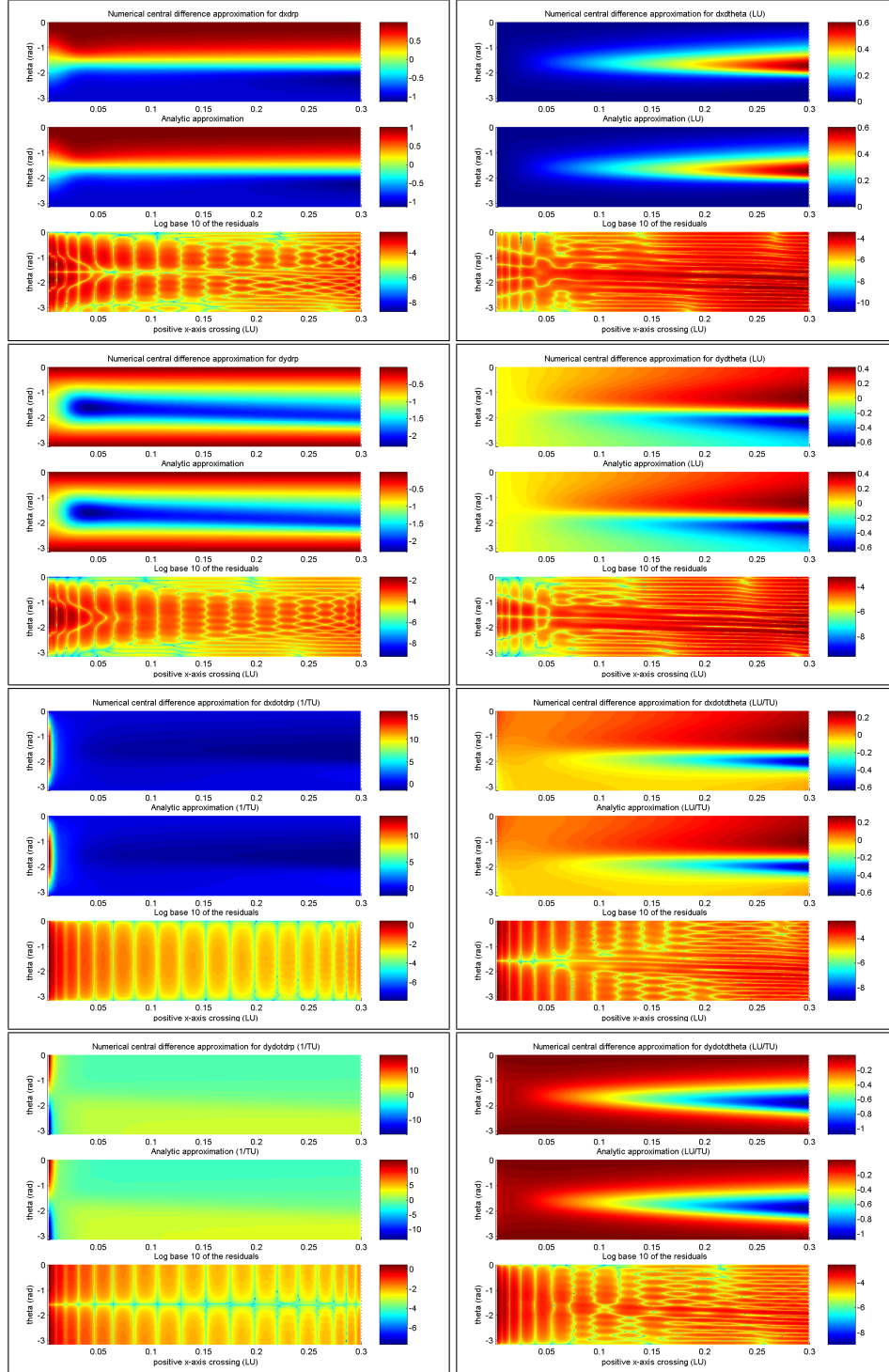


**Figure 7** First derivatives of  $x, y, \dot{x}, \dot{y}$  w.r.t  $r_p$  and  $\theta$  computed using Chebyshev polynomials. The computation is compared against a finite difference computation. The two columns are  $\partial/\partial r_p$  and  $\partial/\partial \theta$ . The rows correspond to  $x, y, \dot{x}, \dot{y}$ . In each box, the first plot is computed using (10), the second using finite differences, and the bottom shows log base 10 of the absolute value of the residual at sample points. The horizontal axis in each plot is  $r_p$  and the vertical axis is  $\theta$ . For this calculation 50 terms of Fourier series and up to degree 100 Chebyshev polynomials were used, i.e., in equation (10)  $M = 50$  and  $N = 100$ .

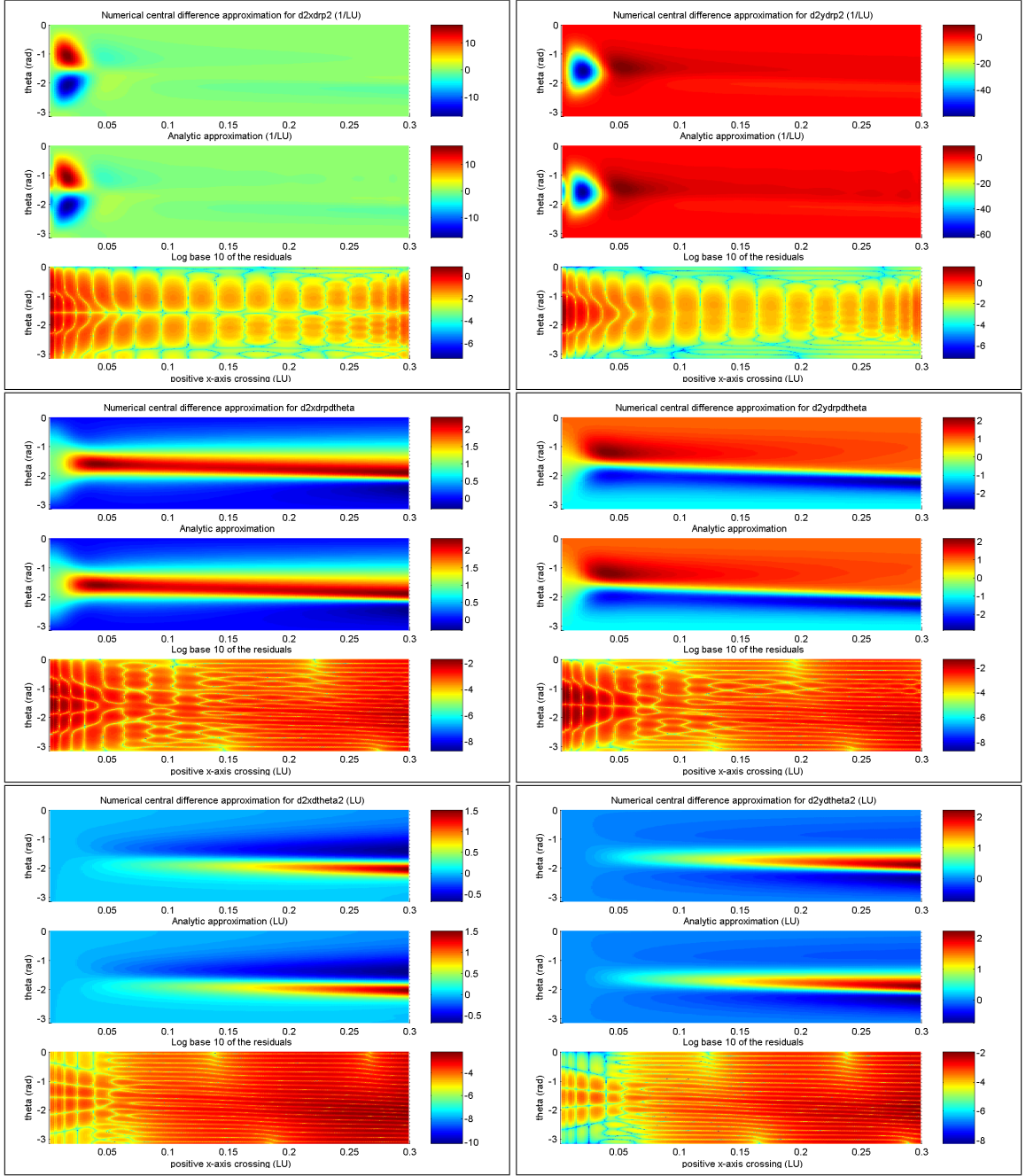
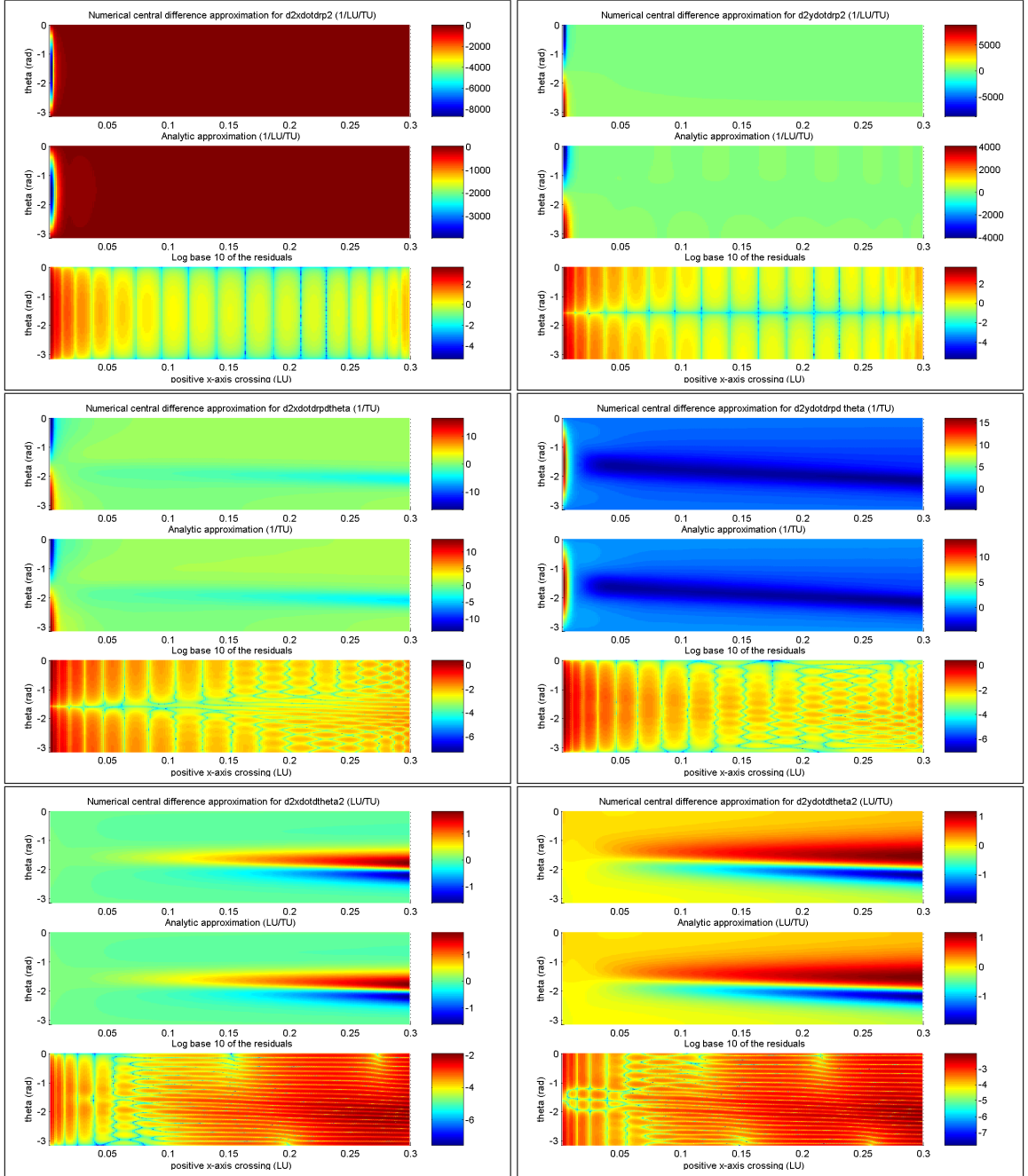


Figure 8 Second derivatives of  $x$   $y$  w.r.t  $r_p$  and  $\theta$  computed using Chebyshev polynomials and compared against a finite difference computation. The left column is for  $x$  and the right one is for  $y$ . The 3 rows correspond to  $\partial^2/\partial r_p^2$ ,  $\partial^2/\partial r_p \partial \theta$  and  $\partial^2/\partial \theta^2$ . In each box, the first plot is computed using (10), the second using finite differences, and the bottom shows log base 10 of the absolute value of the residual at the sample points. The horizontal axis in each plot is  $r_p$  and the vertical axis is  $\theta$ . For this calculation 50 terms of Fourier series and up to degree 100 Chebyshev polynomials were used, i.e., in equation (10)  $M = 50$  and  $N = 100$ .



**Figure 9** Second derivatives of  $\dot{x}$  and  $\dot{y}$  w.r.t  $r_p$  and  $\theta$  computed using Chebyshev polynomials and compared against a finite difference computation. The left column is for  $x$  and the right one is for  $y$ . The 3 rows correspond to  $\partial^2/\partial r_p^2$ ,  $\partial^2/\partial r_p \partial \theta$  and  $\partial^2/\partial \theta^2$ . In each box, the first plot is computed using (10), the second using finite differences, and the bottom shows log base 10 of the absolute value of the residual at the sample points. The horizontal axis in each plot is  $r_p$  and the vertical axis is  $\theta$ . For this calculation 50 terms of Fourier series and up to degree 100 Chebyshev polynomials were used, i.e., in equation (10)  $M = 50$  and  $N = 100$ .